RSC Advances

ROYAL SOCIETY OF CHEMISTRY

www.rsc.org/advances

ARTICLE TYPE www. rsc.org/xxxxxx | XXXXXXXX

Easily prepared ruthenium-complex nanomicelle probes for two-photon quantitative imaging of oxygen in aqueous media

Aamir A. Khan, Susan K. Fullerton-Shirey, and Scott S. Howard*

Received Xth XXXXXXXXXX 20XX, Accepted Xth XXXXXXXXX 20XX
First published on the web Xth XXXXXXXXXX 200X **DOI: 10.1039/b000000x**

We present a simple and inexpensive technique to enable 3D, high-resolution, and quantitative imaging of dissolved oxygen in aqueous media using a commercially available hydrophobic dye, $[Ru(dpp)_3]^{2+}$. The dye is encapsulated in nanomicelles formed by poloxamer (a biocompatible surfactant), allowing for uniform dispersion in aqueous media without long, complex, and expensive chemical synthesis procedures. The nanomicelle probes are tested and found to remain stable for several months in water and for several hours in biological media. The probes are sufficiently large in size for vasculature retention and enable intravenous oxygen imaging *in vivo*. The two-photon cross-section of $[Ru(dpp)_3]^{2+}$ nanomicelle probes surpass that of the well-established and widely used oxygen-sensitive probes in multiphoton microscopy. We also characterize the oxygen-sensitivity of the probes as a proof of their viability as low cost and easily prepared markers for multiphoton quantitative oxygen imaging *in vivo* and other applications in aqueous media.

1 Introduction

Measurement of dissolved oxygen plays an important role in physiological research as well as in many environmental and industrial applications.[1–5] Several areas of medicinal research rely on information about oxygen concentration at the tissue and cellular level. For example, quantitative information about oxygen levels in tumors can lead to optimized treatment methods in oncology.[6] Oxygen imaging of brain vasculature can lead to a better understanding of brain activity in neurological research.[7–10] At the intracellular level, oxygen imaging can provide insights into cellular signaling pathways and metabolic activity.[2,4,11,12]

Measurement of dissolved oxygen can be accomplished either electrochemically or optically. Electrochemical techniques, such as the Clark electrode for example, have the disadvantage of consuming oxygen thus needing constant stirring of the analyte that causes deterioration of the sensing electrode over time.[3,5] In contrast, optical oxygen sensors provide a minimally invasive and non-consuming approach to measure oxygen. These are based on the principle that the photoluminescence from a phosphorescent luminophore depends upon the oxygen concentration in the local microenvironment. Oxygen molecules colliding with an excited luminophore provide a non-radiative pathway for high energy state electrons to relax. This phenomenon, called "collisional quenching" decreases both the phosphorescence intensity and lifetime.[1,13] Either quantity provides a quantitative measurement of oxygen; however, lifetime measurement is preferred because it is self-referencing and relatively less susceptible to light scattering, photobleaching, fluctuations in luminophore concentration, and drift in detector sensitivity and excitation power.[13–15] Lifetime-based techniques are also utilized in fluorescence/phosphorescence lifetime imaging microscopy (FLIM/PLIM), an imaging modality for quantitative measurement of oxygen *in vivo*[7–10,16] and *in vitro*.[4,17]

Most optical oxygen sensors utilize phosphorescent luminophores that are quenchable by oxygen (also called dyes or indicators).[1,2] Examples include porphyrins of platinum and palladium,[18] molybdenum chloride clusters,[5] and ruthenium-complexes such as $[Ru(bpy)_3]^{2+}$ and $[Ru(dpp)_3]^{2+}$.[4,12,15] Even though bioimaging and other aqueous oxygen sensing applications require the dyes to either be water-soluble or be uniformly dispersible in water, the fact is that most of the oxygen-sensitive dyes are hydrophobic in nature.[2,19] To overcome this problem, hydrophobic dyes are usually PEGylated which involves the attachment of hydrophilic functional groups and/or dendrimers to enhance water-solubility.[2,20,21] The Oxyphor family of probes (Oxyphor-R2, -G2, -R4, and -G4) is a good example of changing the hydrophobicity of palladium-porphyrins by adding hydrophilic dendrimers.[22–24] However, the Oxyphor probes lack two-photon cross-section thus cannot be used in multiphoton microscopy[25,26] for high-resolution and depth-resolved bioimaging.[27] Vinogradov *et al.* address this problem through PtP-C343, a hydrophilic dendritic probe with two-photon absorbing antennae attached to a platinum-porphyrin core.[6,28] PtP-C343 is a well-established probe and is widely used in 3D, high-resolution, and quantitative imaging of oxygen *in vivo*,[8–10,16] but requires complex chemical synthesis procedures for preparation.

Department of Electrical Engineering, University of Notre Dame, Notre Dame, IN 46556, USA.; E-mail: showard@nd.edu

Hydrophobic dyes can also be immobilized in an oxygen-permeable polymer matrix (e.g., polystyrene,[29] silicone,[30] polysulfone,[31] etc.) for localized immersion in aqueous media. The immobilizing matrix is usually deposited on a thin film[5,19,30–32] or an optical-fiber tip,[29,33] neither of which enables the uniform dispersion of dye molecules in water. The polymer matrix also adds a barrier between the dye and oxygen molecules, thereby reducing the oxygen-sensitivity and response time.[3] Another technique, PEBBLE nanosensors, encapsulates hydrophobic dyes in organically modified silicate matrices of 100–800 nm size. These nanosensors are prepared by a sol-gel process and are permeable to oxygen.[3,12] In contrast to dendritic/PEGylated probes, PEBBLE nanosensors do not require any chemical synthesis to achieve uniform dispersion of hydrophobic dyes in water.

One of the most important biological applications of oxygen-sensitive probes is oxygen imaging of brain vasculature *in vivo*.[8–10] 3D, high-resolution, and deep brain imaging and other *in vivo* intravenous applications require probes that are: (a) hydrophilic, (b) sufficiently large to be retained within the vasculature, (c) sensitive and permeable to oxygen, (d) compatible with multiphoton microscopy, (e) stable in biological media, and (f) commercially available or easily prepared. However, most water-soluble dyes (e.g., $[Ru(bpy)_3]^{2+}$ and rhodamine B) are small in size and tend to diffuse out of the capillaries into the interstitial fluid. Conjugation with large dextran molecules or grafting with organic luminophores is often required to retain these dyes inside the vasculature.[8,34,35] On the other hand, hydrophilic PEBBLE nanosensors are too large in size (100–800 nm) and pose a greater risk of capillary damage.[3] Only PtP-C343 probe[6,28] fits all the design criteria except that it is not available commercially and requires complex preparation procedures.

In this paper, we present a probe that is simple to prepare and addresses all the requirements for 3D, high-resolution, and quantitative imaging of dissolved oxygen *in vivo*. A low cost, commercially available, oxygen-sensitive, two-photon compatible, and hydrophobic ruthenium-complex dye, $[Ru(dpp)_3]^{2+}$, is encapsulated by the process of surfactant micellization[36] for uniform dispersion in aqueous media. Several methods to solubilize hydrophobic dyes in water through the micelle-encapsulation technique have been reported in the literature.[35,37–39] We adapted a procedure for preparing an *in vivo* vasculature imaging probe,[35] and applied it with several modifications to encapsulate $[Ru(dpp)_3]^{2+}$ for dissolved oxygen imaging in aqueous media. The procedure takes less than two hours and does not involve any laborious and complex chemical synthesis. The dye is first dissolved in chloroform and combined with a solution of surfactant and water. The surfactant, poloxamer-407, is a biocompatible,[40–42] non-ionic A–B–A block copolymer. The B-block is polypropylene oxide (PPO) and the A-block is polyethylene oxide (PEO) as shown in Fig. 1a. Because chloroform is a good solvent for PPO, and water is a good solvent for PEO, nanometer-sized micelles of the surfactant encapsulating the dye are formed when high shear is applied by ultrasonication. The chloroform is evaporated and the solution is filtered to retain only the larger nanomicelles (> 5 nm) that do not diffuse across the vasculature endothelium.[7,35] As shown in Fig. 1b, the nanomicelles sequester the dye in the hydrophobic core while permitting oxygen diffusion, and the hydrophilic tails enable solvation of the surfactant to form a homogenous, aqueous solution.

Qualitative two-photon *in vivo* imaging of mouse brain vasculature have previously been demonstrated using $[Ru(dpp)_3]^{2+}$ and other dyes encapsulated in poloxamer nanomicelles.[7,35] To obtain quantitative results, however, the oxygen-sensitivity of the nanomicelle probes needs to be measured carefully. In this paper, we present the photophysical characterization and show that the probes can be used for quantitative measurements of dissolved oxygen in aqueous media with sensitivity comparable to that of the well-established and widely used probes while providing improved two-photon cross-section. The Stern-Volmer response of the probes is measured and shows larger oxygen-sensitivity than that of $[Ru(dpp)_3]^{2+}$ dissolved in a hydrophobic solvent,[15] $[Ru(dpp)_3]^{2+}$ encapsulated in PEBBLE nanosensors,[12] and comparable to that of PtP-C343.[6,28] The two-photon excitation cross-section of the probes is found to be three times larger than that of PtP-C343[28] and comparable to that of fluorescein.[43] The probes remain stable for several months in water and for several hours in biological media without breaking down, thereby enabling extended time-lapse oxygen imaging *in vivo* and *in vitro*.

2 Preparation of nanomicelle probes

4 mg of $[Ru(dpp)_3]Cl_2$* dye (Alfa Aesar) are dissolved in 100 μL of chloroform. 100 mg of poloxamer-407 surfactant (Pluronic® F127; Sigma-Aldrich) are dissolved in 10 mL deionized (DI) water. A micropipette is used to transfer the dye/chloroform solution to the surfactant/aqueous solution. Because water and chloroform are immiscible, a two-phase mixture forms prior to emulsification. The solution is transferred to a 50 mL plastic centrifuge tube and mounted on a ring stand. An ultrasonic homogenizer (Branson Sonifier® SLPe 150 Watt) with a 1/8 inch diameter microtip is used to create the nanoemulsion. The ultrasonic homogenizer generates the high frequency mechanical energy required to create a stable, homogenous emulsion. The microtip is mounted on a ring stand and lowered into the plastic tube until the tip is immersed in at least 1 cm of solution. The solution is immersed in an ice

* Tris(4,7-diphenyl-1,10-phenanthroline)ruthenium(II) dichloride

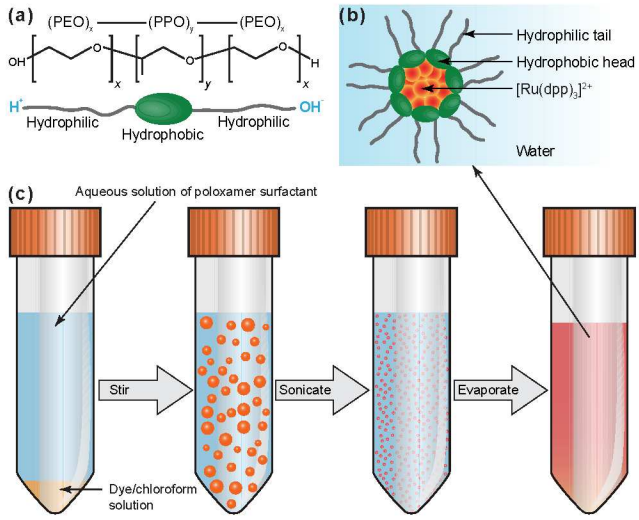

Fig. 1 (a) Structure of poloxamer surfactant block copolymer (PEO–PPO–PEO) highlighting the amphiphilic nature. (b) Structure of the nanomicelles in aqueous media encapsulating $[Ru(dpp)_3]^{2+}$. (c) Step-wise preparation of $[Ru(dpp)_3]^{2+}$ nanomicelle probes.

bath to facilitate rapid cooling and prevent the evaporation of chloroform while the emulsion is formed. The Sonifier® is run continuously for 10 seconds, then turned off for 10 seconds allowing the solution to cool. This sequence is repeated six times at 50% amplitude for a total of 60 seconds of emulsification time. The opacity of the orange solution changes from transparent to opaque when the emulsion is formed. The plastic tube is transferred to a 62 °C water bath for 30 minutes to evaporate the chloroform, leaving a transparent, homogenous orange solution. (Note: phase separation indicates that the emulsification has failed). Aggregates larger than 2.5 μm are removed by passing the solution through Grade 5 Whatman filter paper. Excess surfactant is removed using an Amicon Ultra-15 centrifugal filter (EMD Millipore) with 10 kDa molecular weight cut-off (5 nm pore size). The solution is centrifuged at 5,000 g for 30 minutes using a fixed angle rotor. The faint-orange colored filtrate contains excess water and surfactant, while the deep-orange colored concentrate contains 1.2 mL of $[Ru(dpp)_3]^{2+}$ nanomicelle probe solution (Fig. 1c). The probe solution is stored in a glass vial at room temperature and shows no visual signs of precipitation and/or micelle aggregation for at least 6 months.

2.1 Concentration measurement

In the encapsulation procedure, some amount of $[Ru(dpp)_3]^{2+}$ is lost due to the incomplete mixing of the dye/chloroform and surfactant/water solutions, and the incomplete recovery of smaller nanomicelles (< 5 nm) during centrifugal filtration. The concentration of $[Ru(dpp)_3]^{2+}$ in the nanomicelle solution

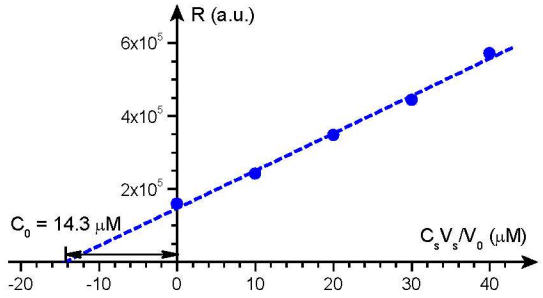

Fig. 2 Standard addition method for determining the concentration of $[Ru(dpp)_3]^{2+}$ in the nanomicelle probes.

will be overestimated if the lost amount is not accounted for. The matrix effect of the encapsulating surfactant further complicates the concentration measurement. To overcome these factors, the method of standard addition[44] is used to measure the concentration of $[Ru(dpp)_3]^{2+}$ in the nanomicelle solution.

Experimental details

Because $[Ru(dpp)_3]Cl_2$ is insoluble in water, a 10 μM solution in methanol is used as the standard for this method. The nanomicelle solution, for which the concentration of $[Ru(dpp)_3]^{2+}$ is sought, is first diluted 100X with DI water before using it as the analyte in this method. Let C_s be the concentration of the standard and C_0 be the unknown concentration of the analyte. Five different samples are prepared by adding equal amounts of the analyte, $V_0 = 0.1$ mL, and progressively increasing amounts of the standard, $V_s = \{0, 0.1, 0.2, 0.3, 0.4\}$ mL, into five separate cuvettes. Each sample is diluted with water until the total volume of the solution in the cuvette reaches 3 mL. Each sample is illuminated by an ultraviolet light emitting diode (UV-LED) and the emission is measured by a photomultiplier tube. The emission response (R) is plotted versus the quantity (C_sV_s/V_0) and fitted to a straight line. The method of standard addition states that the response with no standard ($V_s = 0$) must be due to the analyte, the concentration of which can be determined by extrapolating the straight line as shown in Fig. 2.

Discussion

From the data in Fig. 2, the concentration of the analyte is found to be 14.3 ± 1.28 μM (standard error). Taking into account the dilution factor of 100, this leads to a value of 1430 ± 128 μM as the concentration of $[Ru(dpp)_3]^{2+}$ in the undiluted probe solution. In contrast, only the upper limit of concentration (2851 μM) can be calculated if the lost amount of $[Ru(dpp)_3]^{2+}$ is ignored. This result shows that it is necessary to measure the concentration by standard addition rather than relying on the calculated value.

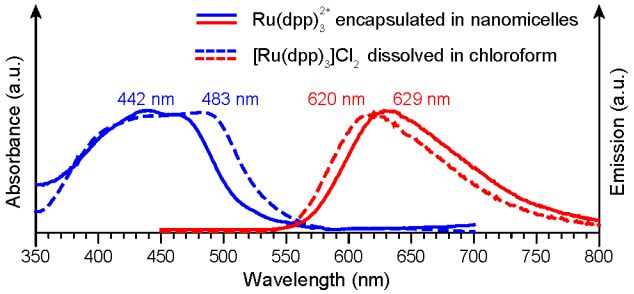

Fig. 3 Absorption and emission spectra of $[Ru(dpp)_3]^{2+}$ nanomicelle aqueous solution compared with those of $[Ru(dpp)_3]Cl_2$ in chloroform. Absorption and emission peaks for $[Ru(dpp)_3]^{2+}$ nanomicelle solution occur at 442 nm and 629 nm respectively and are reasonably close to that of $[Ru(dpp)_3]Cl_2$ in chloroform.

3 Photophysical characterization

It is necessary to show that the nanomicelle probes are effective for quantitative measurement of dissolved oxygen and are compatible with multiphoton microscopy. Four different properties of the probes are thus characterized in the subsequent sections: (a) absorption and emission, (b) sensitivity to dissolved oxygen, (c) two-photon excitation (TPE) cross-section, and (d) stability in various biological media.

3.1 Absorption and emission spectra

Experimental details

Absorption and emission spectra are measured for $[Ru(dpp)_3]^{2+}$ in both hydrophobic and hydrophilic solvents. Two analytes are used for these measurements: (a) $[Ru(dpp)_3]Cl_2$ dissolved in chloroform and (b) $[Ru(dpp)_3]^{2+}$ nanomicelle aqueous solution. The absorption spectra are measured in the range of 350–700 nm with Perkin Elmer Lambda 25 UV/VIS spectrophotometer. The emission spectra are measured with a Horiba Scientific Fluoromax-4 fluorometer. The samples are excited at 425 nm and the emission is scanned in 450–800 nm range.

Discussion

The absorption and emission spectra are presented in Fig. 3 which shows that the encapsulation of $[Ru(dpp)_3]^{2+}$ in poloxamer nanomicelles does not significantly change the spectra. This is reasonable because we would not expect the values of molar absorptivity $(30,000\,M^{-1}cm^{-1})$[45] and emission quantum yield (0.3)[32,46] to change after encapsulation. The peaks are appropriate for linear optical excitation and show compatibility with the existing confocal fluorescence microscopy systems.

3.2 Sensitivity to dissolved oxygen

It is important to confirm that the nanomicelle probes are effective for sensing dissolved oxygen. Therefore, the oxygen-sensitivity is characterized by measuring the phosphorescence lifetime of the probes as a function of dissolved oxygen concentration.

Experimental details

The analyte is prepared by diluting the probe solution in DI water to 10 μM, and transferring to a 1 cm square quartz cuvette for optical excitation. An optical-fiber oxygen sensor (FireSting O_2; Pyro Science) is used as a reference sensor to measure dissolved oxygen in the analyte. A temperature sensor is also installed on the outside wall of the cuvette to monitor the temperature throughout the experiment. The analyte is deoxygenated by flowing nitrogen at a rate of 0.5 $^{L}/_{min}$ through a hypodermic needle lowered into the headspace as shown in Fig. 4a. The gas is not bubbled into the nanomicelle solution directly to avoid excessive foaming of the surfactant. The flow of nitrogen in the headspace slowly displaces all the dissolved oxygen from the analyte. When equilibrium is reached ($pO_2 \approx 0$), nitrogen flow is stopped and the analyte is oxygenated by flowing ambient air until a new equilibrium is reached corresponding to the partial pressure of oxygen in air ($pO_2 \approx 213$ hPa at normal atmospheric pressure of 1013.25 hPa) as shown in Fig. 4d. The analyte is cycled multiple times between the oxygenated and deoxygenated states to demonstrate the lack of hysteresis. The analyte is also continuously stirred using a mini magnetic stir bar to keep the dissolved oxygen concentration uniform throughout the cuvette and to avoid any concentration gradients that might cause a lag between the oxygen sensor reading and the phosphorescence lifetime measurement.

Fig. 4b shows the optical setup used to measure the phosphorescence lifetime (τ) by exciting the nanomicelle solution with an ultraviolet light source and recording the phosphorescence decay through a photon counter. An uncollimated UV-LED (365 nm peak wavelength) illuminates the analyte in the cuvette. As shown in Fig. 4c, the LED is switched by 5 V × 1 μs pulses at a repetition rate of 40 kHz, leaving more than 5 lifetimes ($< 24\,\mu$s) for the emission to decay sufficiently between successive excitation pulses. The phosphorescence from the analyte is collected by an objective lens (Carl-Zeiss EC Plan Neofluar, 10X, 0.3 NA) placed at a right angle to the excitation LED. The phosphorescence is then filtered through two 450 nm longpass UV filters (Thorlabs FEL0450) and detected by a thermoelectrically cooled Hamamatsu H7422PA-40 GaAsP photomultiplier tube (PMT) as outlined in Fig. 4b. All the aforementioned optical components are housed inside a light-tight enclosure so that the optical measurements can be made under dark conditions (< 15 photons per second). A

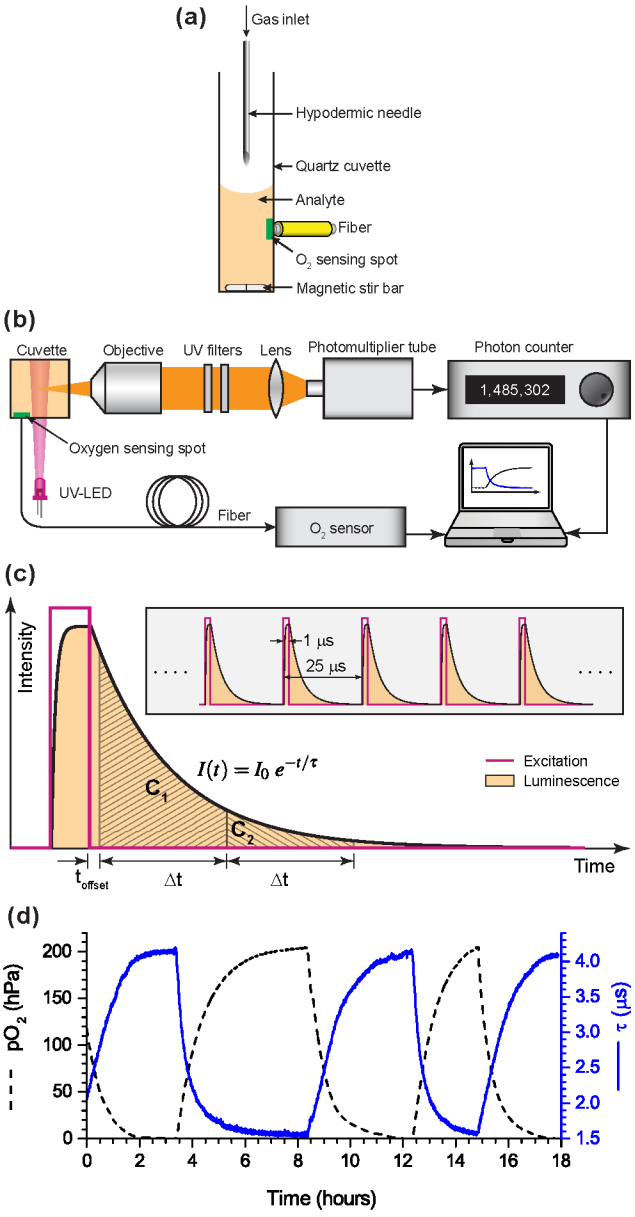

Fig. 4 (a) Setup for oxygenating and deoxygenating the analyte and measuring dissolved oxygen by the reference oxygen sensor. (b) Optical setup for measuring phosphorescence lifetime. (c) Details of rapid lifetime determination (RLD) scheme for lifetime measurement. Pulsed excitation signal for UV-LED in the inset. (d) Partial pressure of oxygen (pO_2) and phosphorescence lifetime (τ) as the analyte is alternately oxygenated and deoxygenated. pO_2 is measured with the fiber-optic oxygen sensor and τ is measured with the photon counter.

photon counter (Stanford Research Systems SR400) is connected to the PMT output and controlled remotely through custom scripts written in MATLAB®. Lifetime is measured using the rapid lifetime determination (RLD) method as the analyte is being oxygenated and deoxygenated. As shown in Fig. 4c, the RLD scheme divides the emission decay profile into two gates of equal width (Δt) and uses the intensity ratio (C_1/C_2) to calculate τ according to the following equation,

$$\tau = \frac{\Delta t}{\ln(C_1/C_2)} \quad (1)$$

To account for the non-zero turn-off time of the excitation pulse, opening of the first gate is delayed by a small amount, $t_{offset} = 0.5\ \mu s$, before starting the RLD measurement. Shot noise in photon statistics introduces error in the lifetime value obtained from the RLD method. As shown by Ballew and Demas, the error can be minimized by setting the gate widths to 2.5τ.[47] Thus to minimize the error, the gate widths are adjusted for each RLD measurement as τ changes during the course of the experiment. Even in the absence of shot noise, the RLD scheme yields the true value of lifetime only when the decay profile is perfectly monoexponential. For multiexponential decay, however, only an effective lifetime value that is indicative of the multiple rates in the luminescence decay process, can be obtained. Nevertheless, because multiexponential decay is a characteristic of the probe and will be manifested all the times under similar conditions, the nanomicelle probes can be characterized in terms of effective lifetime and reliable measurements of oxygen partial pressure can be made.[14]

Discussion

The Stern-Volmer relationship describes the collisional quenching of phosphorescence by oxygen molecules as,

$$\frac{\tau_0}{\tau} = 1 + K_{SV}\, pO_2 \quad (2)$$

where τ is the phosphorescence lifetime at a partial pressure of oxygen (pO_2), τ_0 is the lifetime in the absence of oxygen ($pO_2 = 0$) and K_{SV} is the pressure-based Stern-Volmer constant. This equation represents a straight line with a slope of K_{SV} and an offset of 1. The measured dataset, (pO_2, τ) from Fig. 4d, is least-squares fitted to Eq. (2) in order to determine the Stern-Volmer parameters (τ_0 and K_{SV}) for $[Ru(dpp)_3]^{2+}$ nanomicelle probes as shown in Fig. 5a. Because the quenching of phosphorescence by oxygen is also a function of temperature, the analyte is kept at an average temperature of 24.8 °C (standard deviation of ±0.9 °C) during the experiment. Based on the results reported by Morris *et al.* for $[Ru(dpp)_3]^{2+}$ dissolved in ethylene glycol,[15] it is calculated that a temperature variation of ±0.9 °C will introduce a fractional error of no more than ±0.5% in τ_0 and ±3% in K_{SV}.

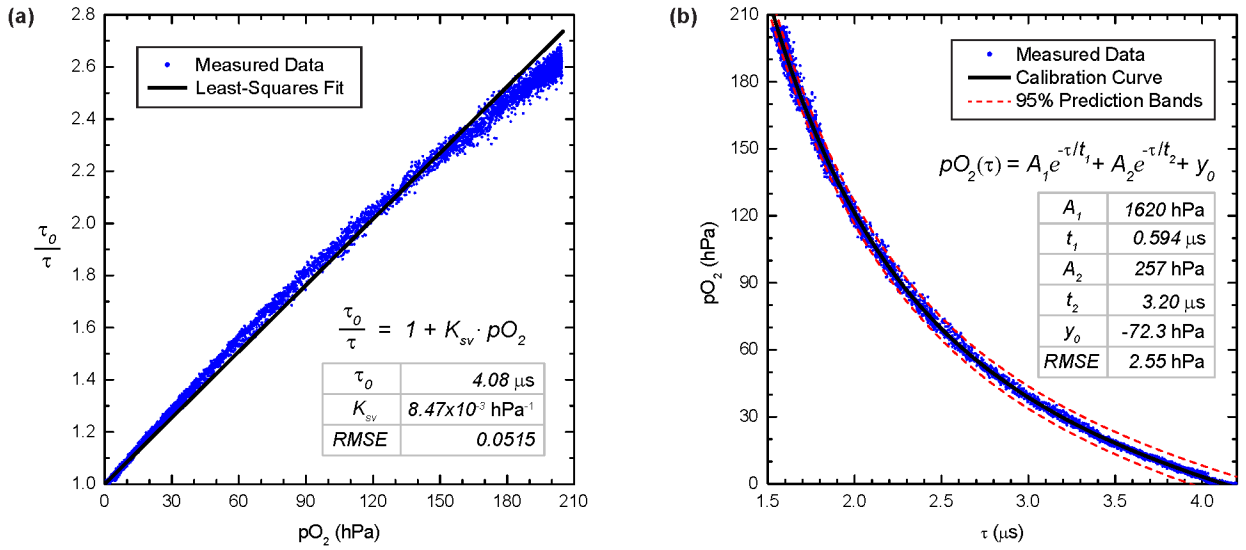

Fig. 5 (a) The Stern-Volmer plot and (b) the calibration curve of $[Ru(dpp)_3]^{2+}$ nanomicelle probes in aqueous solution obtained by fitting the measured data to Eq. (2) and (3) respectively. The measured dataset consists of 6,334 points collected from multiple cycles of oxygenation and deoxygenation (Fig. 4d) within a temperature range of $24.8 \pm 0.9\,^{\circ}C$. Fitting parameters and the root mean square error (RMSE) are shown for both the fits.

This level of error is considered acceptable in an initial proof-of-concept study to show that $[Ru(dpp)_3]^{2+}$ retains sensitivity to dissolved oxygen after encapsulation in poloxamer nanomicelles.

Oxygen-sensitivity of the probe is directly related to the Stern-Volmer constant (K_{SV}), therefore a larger value results in a wider dynamic range and a better contrast in imaging applications.[1] However, an exceedingly large value of K_{SV} is also undesirable because it requires a lifetime measurement setup of extended dynamic range and also deteriorates the signal-to-noise performance at high values of oxygen partial pressure (pO_2). Other important design parameters for *in vivo* imaging probes are water-solubility and large particle size (10–100 nm) for vasculature retention.[35] Two-photon excitation is also required for high-resolution and deep (~ 1 mm) 3D imaging *in vivo*.[48] Table 1 compares several oxygen-sensitive probes and shows that apart from this work, only PtP-C343 probe[6,28] fits all these criteria for two-photon imaging of dissolved oxygen *in vivo*. However, as mentioned in Sec. 1, PtP-C343 requires complex synthesis procedures in contrast to the easy preparation of $[Ru(dpp)_3]^{2+}$ nanomicelle probes. When compared among water-soluble and two-photon compatible probes, the oxygen-sensitivity of $[Ru(dpp)_3]^{2+}$ nanomicelle probes is comparable to that of PtP-C343,[28] and larger than that of both $[Ru(dpp)_3]^{2+}$ encapsulated in PEBBLE nanosensors[12] and the hydrophilic dye, $[Ru(bpy)_3]^{2+}$.[15]

As evident in Fig. 5a, the Stern-Volmer plot of the nanomicelle probes deviates from a straight line and exhibits a concave curvature. This phenomenon is well known for the encapsulated probes and is caused by the nonuniform access of oxygen molecules to the encapsulated dye.[12,30,32,49] Nevertheless, the reproducibility of the oxygen sensing response remains unaffected.[28] For calibration purposes, however, another equation is needed in order to represent the observed response of $[Ru(dpp)_3]^{2+}$ nanomicelle probes with minimal error. Fig. 5b shows the measured data fitted to an empirical biexponential decay model,[8,10,50]

$$pO_2(\tau) = A_1 e^{-\tau/t_1} + A_2 e^{-\tau/t_2} + y_0 \qquad (3)$$

using a least-squares fitting algorithm. The root mean square error (RMSE) between this calibration curve (Eq. 3) and the measured dataset of 6,334 data points is 2.55 hPa (1.25% of full scale). The data are collected over a course of 18 hours in multiple cycles of oxygenation and deoxygenation (Fig. 4d). This clearly demonstrates the repeatability and the lack of hysteresis in the oxygen sensing response of the nanomicelle probes. The small spread in the measured datapoints (Fig. 5b) can be attributed to the temperature variations during the experiment ($\pm 0.9\,^{\circ}C$). Planned future work aims to study the effect of temperature on the oxygen-sensitivity of the probes.

It is to be noted that the values of K_{SV} and calibration constants depend on the chemistry of the medium.[23] Thus, the characterization of the oxygen sensing response of $[Ru(dpp)_3]^{2+}$ nanomicelle probes, as shown in Fig. 5, is only valid in water. Future work is planned to generate calibration curves for using the probes in biological media. Nevertheless, the calibration in aqueous solution serves to show that

Table 1 Comparison of oxygen sensing probes from the literature

Probes	K_{SV} ($\times 10^{-3}$ hPa^{-1})	Water solubility	Vasculature retention	Two-photon excitation
$[Ru(dpp)_3]^{2+}$ nanomicelle probes	8.47	✓	✓	✓
PtP-C343 (dendritic Pt-porphyrin)[28]	7.65	✓	✓	✓
Oxyphor-R2 (dendritic Pd-porphyrin)[22]	155*	✓	✓	
Oxyphor-G2 (dendritic Pd-porphyrin)[22]	39.6	✓	✓	
Oxyphor-R4 (dendritic Pd-porphyrin)[23]	37.3	✓	✓	
Oxyphor-G4 (dendritic Pd-porphyrin)[23]	34.5	✓	✓	
PtOEPK PEBBLE nanosensors[3]	32.6	✓	✓‡	
$[Ru(dpp)_3]^{2+}$ PEBBLE nanosensors[12]	3.94	✓	✓‡	✓
$[Ru(bpy)_3]^{2+}$ dissolved in water[15]	2.47	✓		✓
$[Ru(dpp)_3]^{2+}$ dissolved in ethylene glycol[15]	6.72			✓
$[Ru(dpp)_3]^{2+}$ immobilized in silicone[30]	30.1			✓
$K_2Mo_6Cl_{14}$ immobilized in silicone[5]	9.62			✓

* Probes with large K_{SV} values have a poor signal-to-noise performance at high oxygen levels and require a measurement setup with extended dynamic range.
‡ Large particle sizes (100–800 nm) pose a greater risk of capillary damage.[3]

$[Ru(dpp)_3]^{2+}$ remains sensitive to oxygen after encapsulation in poloxamer nanomicelles.

3.3 Two-photon excitation cross-section spectrum

Two-photon luminescence is a nonlinear optical phenomenon which is directly proportional to the squared excitation intensity ($F \propto P^2$). This phenomenon induces luminescence in a diffraction-limited and depth-resolved focal point to construct 3D images without a pinhole as required by confocal microscopy.[25] The two-photon excitation cross-section (σ_{TPE}) of a probe is defined as the product of two-photon luminescence quantum yield (η_2) and two-photon absorption cross-section (σ_{TPA}),

$$\sigma_{TPE} = \eta_2 \sigma_{TPA} \tag{4}$$

A large value of two-photon excitation (TPE) cross-section is desired because this enables deeper penetration and higher signal-to-noise ratio in 3D multiphoton imaging.

Experimental details

We employ a ratiometric method[51] to measure the TPE cross-section spectrum of $[Ru(dpp)_3]^{2+}$ nanomicelle probes. Fluorescein (10 μM, pH 11 in aqueous NaOH) is used as a two-photon cross-section standard. The analyte (50 μM solution of $[Ru(dpp)_3]^{2+}$ nanomicelles) is placed in a quartz cuvette where nitrogen or air is kept flowing in the headspace to equilibrate the dissolved oxygen concentration (pO_2) with either 0 or 213 hPa as monitored by a fiber-optic oxygen sensor (FireSting O_2; Pyro Science). A custom-built two-photon fluorospectrometer is used to perform the two-photon cross-section measurements as outlined in Fig. 6. A mode-locked Ti:sapphire laser (Spectra Physics Mai Tai BB, 710–990 nm, 100 fs pulse width, 80 MHz repetition rate) is used to induce two-photon excited luminescence in fluorescein and $[Ru(dpp)_3]^{2+}$ nanomicelle probes. The laser power is controlled by a variable neutral-density filter and the beam is filtered through a 664 nm longpass filter (Semrock Inc.) to block ambient room light from entering into a light-tight enclosure, housing the analyte and the detector. The laser beam is expanded through L_1 and L_2 to overfill the back aperture of an objective lens (Olympus Plan Achromat, 4X, 0.1 NA) which creates a diffraction-limited spot inside the cuvette. The two-photon excited luminescence is epi-collected by the same objective lens and is directed towards a photomultiplier tube (Hamamatsu H7422PA-40) by a 700 nm dichroic mirror (Chroma Technology Corp.). The luminescence is filtered through a set of 315–710 nm bandpass colored glass filter (Thorlabs FGS900) and two 700 nm shortpass dielectric filters (Chroma Technology Corp.) to keep any residual excitation from reaching the detector. The luminescence (F) is detected by the photomultiplier tube and measured by a photon counter (Stanford Research Systems SR400). A mechanized arm switches between the cuvette and an optical power meter (Thorlabs S120C) to measure the excitation power (P) at the focal spot.

Six readings are taken at each excitation wavelength (710–990 nm in 10 nm steps) for the three samples: (a) fluorescein as the standard, (b) air-saturated nanomicelle solution, and (c) deoxygenated nanomicelle solution. For each reading, the neutral density filter is adjusted and the mechanized arm brings the power sensor to focus to measure P. Later, the power sensor is removed and the cuvette is focused to measure F. An objective lens of low numerical aperture (0.1) is used to avoid luminescence saturation. Furthermore, the strict quadratic dependence of two-photon luminescence ($F = aP^2$)

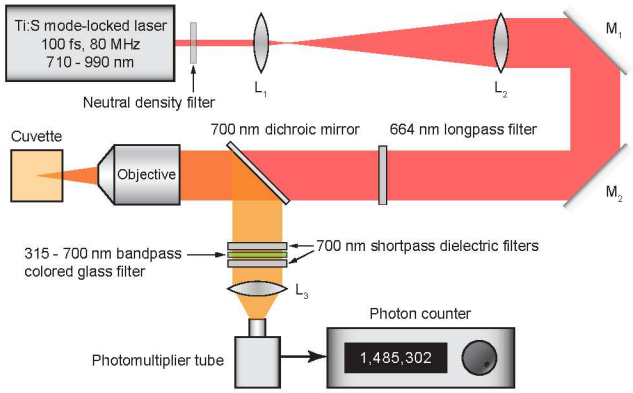

Fig. 6 Two-photon fluorospectrometer for measuring the two-photon excitation cross-section spectrum.

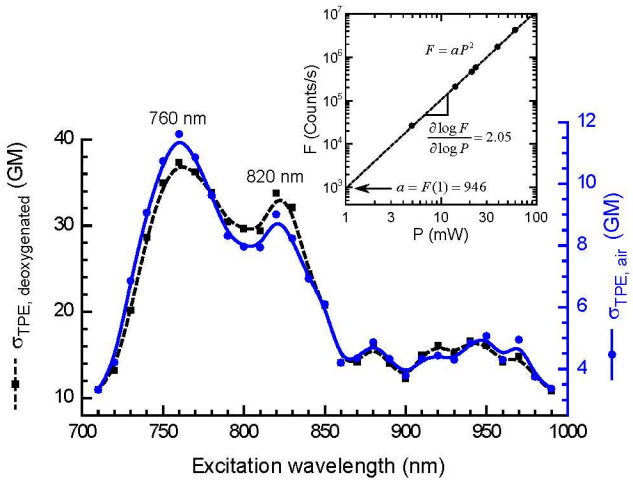

Fig. 7 Two-photon excitation cross-section spectrum of $[Ru(dpp)_3]^{2+}$ nanomicelle probes. The spectrum peaks at 760 nm and shows an extinction ratio of 3.2 between air-saturated ($pO_2 \approx 213$ hPa) and deoxygenated ($pO_2 \approx 0$) conditions. The readings are taken at 10 nm intervals and the lines are drawn only as a guide to the eye. Inset: Two-photon luminescence (F) versus excitation (P) curve showing the strict quadratic dependence and the curve fitting scheme to determine the coefficient 'a'.

is confirmed at each wavelength over an extended range of excitation power (6–60 mW, corresponding to 75–750 pJ of pulse energy). The inset of Fig. 7 shows a representative set of such readings where the coefficient of quadratic dependence (a) is obtained by fitting the six data points to the linear equation, $\log F = \log a + 2 \log P$. After determining the coefficients '$a(\lambda)$' at each wavelength for all the three samples, the TPE cross-section spectrum can be calculated according to the ratiometric method as,[51]

$$\sigma_{TPE-r}(\lambda) = \sigma_{TPE-s}(\lambda) \frac{a_r(\lambda)}{a_s(\lambda)} \frac{\Phi_s n_s C_s}{\Phi_r n_r C_r} \quad (5)$$

where the subscripts 'r' and 's' denote the $[Ru(dpp)_3]^{2+}$ nanomicelle solution and the standard solution (fluorescein) respectively, σ_{TPE} is the TPE cross-section, Φ is the collection efficiency of the optical system, and C and n are the concentration and the refractive index of the luminophore solution respectively. The refractive indices are assumed to be equal while the collection efficiencies are measured by convolving the emission spectrum of the respective luminophore with the transmission spectrum of the detection path and the spectral response of the photomultiplier tube.

Discussion

As presented in Sec. 2.1, the concentration of $[Ru(dpp)_3]^{2+}$ in the nanomicelle probes (C_r) was measured with a standard error of ±9%. Propagating this error along with an error of ±30% in the standard dataset (σ_{TPE-s}) through Eq. 5, results in an error of ±31% in the TPE cross-section of $[Ru(dpp)_3]^{2+}$ nanomicelle probes (σ_{TPE-r}).[43,54] The error in the absolute values is due largely to the error in the standard dataset; however, the spectral shape and the TPE cross-section values relative to fluorescein[43] are much more accurate and give insight into how to use the nanomicelle probes for two-photon microscopy. The TPE cross-section peaks at 760 nm with a value of 37.3 GM and 11.6 GM for deoxygenated and air-saturated conditions respectively. (Note: 1 GM = 10^{-50} cm^4 s photon^{-1}). As shown in Table 2, the TPE cross-section of $[Ru(dpp)_3]^{2+}$ nanomicelle probes is comparable to or larger than that of the widely used probes in multiphoton microscopy such as Fluorescein[43] and the oxygen-sensitive probe, PtP-C343.[28]

3.4 Stability in biological media

The poloxamer nanomicelles are formed by the hydrophobic-hydrophilic equilibrium of PPO and PEO blocks in water (Fig. 1a & 1b).[55] Even though the nanomicelle probes are visually confirmed to be stable in DI water without any signs of precipitation and/or micelle aggregation for over 6 months, the presence of other chemical species in the aqueous solution, especially ions, can potentially disturb this equilibrium and cause the nanomicelles to break (demicellize), leading to phase separation.[56] As the nanomicelles demicellize, the hydrophobic $[Ru(dpp)_3]^{2+}$ molecules in the cores can no longer remain suspended in the aqueous solution.[36] Thus it is important to characterize the stability of the probes in biological media of interest.

Experimental details

The nanomicelle probes are tested for stability in six different media: (a) deionized (DI) water, (b) 5% solution of bovine

Table 2 Comparison of TPE cross-sections of several two-photon imaging probes

Luminophore	σ_{TPE} (GM)	η_2	λ (nm)
$[Ru(dpp)_3]^{2+}$ nanomicelle probes	37.3 ± 11.7	0.3 [32,46]	760
PtP-C343 (dendritic Pt-porphyrin)	13 (calculated value) [28]	0.1 [28]	840
Fluorescein	34 ± 8.7 [43]	0.9 [52]	782
Rhodamine B	105 ± 28 [43]	0.5 [53]	840

serum albumin (BSA; Sigma-Aldrich) in DI water, (c) 5% solution of BSA in phosphate buffered saline (PBS-1X, pH 7.4; Sigma-Aldrich), (d) wild-type mouse blood diluted 20X with PBS-1X, (e) McCoy's 5A growth medium (with L-glutamine and sodium bicarbonate; Sigma-Aldrich), and (f) PBS-1X. Note that the mouse blood is diluted 20X with PBS-1X because of the turbidity of the blood; dilution makes the optical measurements possible while keeping the pH and the electrolyte concentration similar to that of undiluted blood. Each analyte is prepared by mixing 0.2 mL of $[Ru(dpp)_3]^{2+}$ nanomicelle solution (150 μM) with 2.8 mL of the respective solvent medium. Samples (a) and (f) are excited by a UV-LED, while samples (b), (c), (d), and (e) by a mode-locked Ti:S laser (two-photon excitation at 820 nm) to avoid the endogenous fluorescence of amino acids and proteins. The excitation source serves only to induce phosphorescence in the analyte and does not change the probe demicellization rate. The emission is collected by a photomultiplier tube, and is proportional to the concentration of encapsulated $[Ru(dpp)_3]^{2+}$ molecules in the nanomicelle solution. The data are collected for several hours, and a steady drop in the emission intensity is observed corresponding to the probe demicellization as shown in Fig. 8.

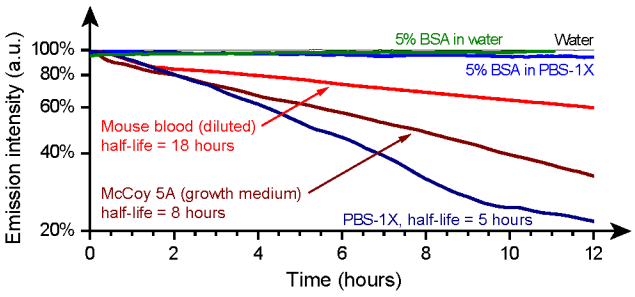

Fig. 8 The emission intensity and correspondingly the probe concentration diminishes as the nanomicelles break down in biological media over time. The shortest half-life of the probe demicellization is 5 hours in PBS-1X and readily exceeds the time required for *in vivo* imaging. (Note: The vertical axis is logarithmic).

Discussion

The data in Fig. 8 show that the nanomicelle probes are especially stable in DI water and solutions of bovine serum albumin in DI water and PBS. One commonality among these three media is a lower pH ($\sim$ 4–6) compared to mouse blood, growth medium, and PBS-1X (pH 7.4). However, regardless of the media, the stability of the nanomicelle probes exceed the time required for *in vivo* imaging experiments. [35] To determine the half-lives of the probe demicellization in the three media at a physiologically relevant pH of 7.4, the emission data are fitted to a monoexponetial decay function. Data fitting yield half-lives of 18, 8, and 5 hours in mouse blood, growth medium, and PBS, respectively. In addition to a higher pH, these media contain electrolytes which are known to lower the cloud point of poloxamer nanomicelles. [36,56]

The stability data presented in Fig. 8 are collected at room temperature. At higher temperature, poloxamer micelles tend to aggregate, leading to increased solution viscosity. [57] Therefore, the use of $[Ru(dpp)_3]^{2+}$ nanomicelle probes at a physiologically relevant temperature (37 °C) is not expected to increase the demicellization rate; however, the effect of micelle aggregation on performance as an oxygen sensing probe will require further investigation.

4 Conclusions

We have demonstrated a simple and low cost procedure of preparing a hydrophobic phosphorescence dye, $[Ru(dpp)_3]^{2+}$, for quantitative imaging of dissolved oxygen in aqueous media. The procedure requires less than two hours to prepare the nanomicelle probes which remain stable for several months in water. The probes remain stable in biological media for several hours readily exceeding the time required for *in vivo* imaging. The surfactant used for encapsulation, Pluronic® F127 (poloxamer-407), is also biocompatible [40–42] thus making the nanomicelle probes an attractive choice for quick and inexpensive bioimaging applications.

We have also described the experimental techniques to characterize the oxygen sensing response of any phosphorescence dye for a wide range of oxygen conditions (0–213 hPa). $[Ru(dpp)_3]^{2+}$ nanomicelle probes show at least twice as much sensitivity to dissolved oxygen than that of $[Ru(bpy)_3]^{2+}$ dissolved in water, [15] $[Ru(dpp)_3]^{2+}$ encapsulated in PEBBLE nanosensors, [12] and comparable to that of the state-of-the-art oxygen imaging probe, PtP-C343. [6,28] Because the phenomena

of phosphorescence emission and phosphorescence quenching by oxygen are both independent of the pathway by which the luminophore is promoted to the excited state, the Stern-Volmer and the calibrations parameters measured under linear (ultraviolet) excitation (Fig. 5) are also valid for oxygen measurement with two-photon excitation.[6,8] The probes are also compatible with multiphoton microscopy, showing a three times larger two-photon excitation cross-section than that of PtP-C343[28] and comparable to that of fluorescein.[43]

The nanomicelle probes, however, have a few shortcoming as well. $[Ru(dpp)_3]^{2+}$, though inexpensive, suffers from photobleaching and has a temperature-dependent oxygen sensing response. To be used as an *in vivo* oxygen imaging probe, both the temperature and solvent dependent calibration curves for oxygen-sensitivity need to be measured. Even with these fundamental limitations, the experimental results demonstrate that $[Ru(dpp)_3]^{2+}$ nanomicelle probes are comparably sensitive to dissolved oxygen and are also suitable for two-photon oxygen imaging of vasculature *in vivo*.[7] Future work with the nanomicelle probes aims to study *in vivo* stability, size distribution of nanomicelles, temperature dependence of oxygen-sensitivity, oxygen monitoring in cell culture medium, and two-photon *in vivo* imaging of mouse ischemia models.

Acknowledgments

The authors would like to thank Dr. Sergei Vinogradov (School of Medicine, University of Pennsylvania) and Dr. Ruby Ghosh (Department of Physics & Astronomy, Michigan State University) for helpdul discussions on oxygen-sensitive optical probes and gas dissolving techniques. Aamir A. Khan is supported by a graduate fellowship in Advanced Diagnostics & Therapeutics from Berry Family Foundation (Dayton, Ohio, USA). Susan K. Fullerton-Shirey acknowledges support from Notre Dame Center for Nanoscience and Technology (NDnano).

References

1 D. B. Papkovsky and R. I. Dmitriev, *Chemical Society Reviews*, 2013, **42**, 8700–32.
2 M. Quaranta, S. M. Borisov and I. Klimant, *Bioanalytical Reviews*, 2012, **4**, 115–157.
3 Y.-E. L. Koo, Y. Cao, R. Kopelman, S. M. Koo, M. Brasuel and M. A. Philbert, *Analytical Chemistry*, 2004, **76**, 2498–505.
4 W. Zhong, P. Urayama and M.-A. Mycek, *Journal of Physics D: Applied Physics*, 2003, **36**, 1689–95.
5 R. N. Ghosh, P. A. Askeland, S. Kramer and R. Loloee, *Applied Physics Letters*, 2011, **98**, 221103.
6 O. S. Finikova, A. Y. Lebedev, A. Aprelev, T. Troxler, F. Gao, C. Garnacho, S. Muro, R. M. Hochstrasser and S. A. Vinogradov, *ChemPhysChem*, 2008, **9**, 1673–79.
7 S. S. Howard, A. Straub, N. G. Horton, D. Kobat and C. Xu, *Nature Photonics*, 2013, **7**, 33–37.
8 S. Sakadzić, E. Roussakis, M. A. Yaseen, E. T. Mandeville, V. J. Srinivasan, K. Arai, S. Ruvinskaya, A. Devor, E. H. Lo, S. A. Vinogradov and D. A. Boas, *Nature Methods*, 2010, **7**, 755–9.
9 J. Lecoq, A. Parpaleix, E. Roussakis, M. Ducros, Y. G. Houssen, S. A. Vinogradov and S. Charpak, *Nature Medicine*, 2011, **17**, 893–8.
10 S. M. S. Kazmi, A. J. Salvaggio, A. D. Estrada, M. A. Hemati, N. K. Shaydyuk, E. Roussakis, T. A. Jones, S. A. Vinogradov and A. K. Dunn, *Biomedical Optics Express*, 2013, **4**, 1061–73.
11 D. F. Wilson, O. S. Finikova, A. Y. Lebedev, S. Apreleva, A. Pastuszko, W. M. F. Lee and S. A. Vinogradov, in *Oxygen Transport to Tissue XXXII*, ed. J. C. LaManna, M. A. Puchowicz, K. Xu, D. K. Harrison and D. F. Bruley, Springer US, 2011, vol. 701, pp. 53–59.
12 H. Xu, J. W. Aylott, R. Kopelman, T. J. Miller and M. A. Philbert, *Analytical Chemistry*, 2001, **73**, 4124–33.
13 H. C. Gerritsen, A. Draaijer, D. J. Heuvel and A. V. Agronskaia, in *Handbook Of Biological Confocal Microscopy*, ed. J. B. Pawley, Springer US, 3rd edn., 2006, pp. 516–534.
14 M. I. J. Stich, L. H. Fischer and O. S. Wolfbeis, *Chemical Society Reviews*, 2010, **39**, 3102–14.
15 K. J. Morris, M. S. Roach, W. Xu, J. N. Demas and B. A. DeGraff, *Analytical Chemistry*, 2007, **79**, 9310–4.
16 J. A. Spencer, F. Ferraro, E. Roussakis, A. Klein, J. Wu, J. M. Runnels, W. Zaher, L. J. Mortensen, C. Alt, R. Turcotte, R. Yusuf, D. Côté, S. A. Vinogradov, D. T. Scadden and C. P. Lin, *Nature*, 2014, **508**, 269–73.
17 H. C. Gerritsen, R. Sanders, A. Draaijer, C. Ince and Y. K. Levine, *Journal of Fluorescence*, 1997, **7**, 11–15.
18 D. B. Papkovsky, G. V. Ponomarev, W. Trettnak and P. O'Leary, *Analytical Chemistry*, 1995, **67**, 4112–7.
19 C. O'Donovan, J. Hynes, D. Yashunski and D. B. Papkovsky, *Journal of Materials Chemistry*, 2005, **15**, 2946.
20 D. Horn and J. Rieger, *Angewandte Chemie International Edition*, 2001, **40**, 4330–4361.
21 U. Hahn, H. Luelf, H. D. F. Winkler, C. a. Schalley, F. Vögtle and L. De Cola, *Chemistry – A European Journal*, 2012, **18**, 15424–32.
22 I. Dunphy, S. A. Vinogradov and D. F. Wilson, *Analytical Biochemistry*, 2002, **310**, 191–198.
23 T. V. Esipova, A. Karagodov, J. Miller, D. F. Wilson, T. M. Busch and S. A. Vinogradov, *Analytical Chemistry*, 2011, **83**, 8756–65.
24 S. A. Vinogradov and D. F. Wilson, in *Oxygen Transport to Tissue XIX*, ed. D. K. Harrison and D. T. Delpy, Springer US, 1997, vol. 428, pp. 657–662.
25 W. R. Zipfel, R. M. Williams and W. W. Webb, *Nature Biotechnology*, 2003, **21**, 1369–77.
26 W. Denk, J. Strickler and W. Webb, *Science*, 1990, **248**, 73–76.
27 M. A. Yaseen, V. J. Srinivasan, S. Sakadzić, W. Wu, S. Ruvinskaya, S. A. Vinogradov and D. A. Boas, *Optics Express*, 2009, **17**, 22341–50.
28 A. Y. Lebedev, T. Troxler and S. A. Vinogradov, *Journal of Porphyrins and Phthalocyanines*, 2008, **12**, 1261–69.
29 I. Klimant, V. Meyer and M. Kuhl, *Limnology and Oceanography*, 1995, **40**, 1159–1165.
30 J. R. Bacon and J. N. Demas, *Analytical Chemistry*, 1987, **59**, 2780–2785.
31 D. Badocco, A. Mondin, P. Pastore, S. Voltolina and S. Gross, *Analytica Chimica Acta*, 2008, **627**, 239–46.
32 A. Mills and M. Thomas, *The Analyst*, 1997, **122**, 63–68.
33 P. Jorge, C. Maule, A. Silva, R. Benrashid, J. Santos and F. Farahi, *Analytica Chimica Acta*, 2008, **606**, 223 – 229.
34 A. C. Kreitzer, K. R. Gee, E. A. Archer and W. G. Regehr, *Neuron*, 2000, **27**, 25–32.
35 M. Maurin, O. Stéphan, J.-C. Vial, S. R. Marder and B. van der Sanden, *Journal of Biomedical Optics*, 2011, **16**, 036001.
36 P. Alexandridis and T. A. Hatton, *Colloids and Surfaces A: Physicochemical and Engineering Aspects*, 1995, **96**, 1–46.

37 M. Maurin, L. Vurth, J.-C. Vial, P. Baldeck, S. R. Marder, B. Van der Sanden and O. Stephan, *Nanotechnology*, 2009, **20**, 235102.

38 C. D. Andrade, C. O. Yanez, M. A. Qaddoura, X. Wang, C. L. Arnett, S. A. Coombs, J. Yu, R. Bassiouni, M. V. Bondar and K. D. Belfield, *Journal of Fluorescence*, 2011, **21**, 1223–30.

39 A. Tehrani-Bagha and K. Holmberg, *Materials*, 2013, **6**, 580–608.

40 Y. Shachaf, M. Gonen-Wadmany and D. Seliktar, *Biomaterials*, 2010, **31**, 2836–2847.

41 W. Hennink, E. V. Batrakova and A. V. Kabanov, *Journal of Controlled Release*, 2008, **130**, 98–106.

42 G. Riess, *Progress in Polymer Science*, 2003, **28**, 1107–1170.

43 C. Xu and W. Webb, *Journal of the Optical Society of America B*, 1996, **13**, 481–491.

44 D. C. Harris, *Quantitative Chemical Analysis*, W. H. Freeman, New York, 6th edn., 2003.

45 G. A. Crosby and R. J. Watts, *Journal of the American Chemical Society*, 1971, **93**, 3184–3188.

46 K. Nakamaru, K. Nishio and H. Nobe, *The Science Reports of the Hirosaki University*, 1979, **26**, 57–62.

47 R. M. Ballew and J. N. Demas, *Analytical Chemistry*, 1989, **61**, 30–33.

48 F. Helmchen and W. Denk, *Nature Methods*, 2005, **2**, 932–40.

49 J. Demas, B. DeGraff and W. Xu, *Analytical Chemistry*, 1995, **67**, 1377–80.

50 S. Sakadzić, S. Yuan, E. Dilekoz, S. Ruvinskaya, S. A. Vinogradov, C. Ayata and D. A. Boas, *Applied Optics*, 2009, **48**, D169–77.

51 M. A. Albota, C. Xu and W. W. Webb, *Applied Optics*, 1998, **37**, 7352–6.

52 G. A. Crosby and J. N. Demas, *The Journal of Physical Chemistry*, 1971, **75**, 991–1024.

53 T. Karstens and K. Kobs, *The Journal of Physical Chemistry*, 1980, **84**, 1871–1872.

54 NIH-NIBIB Biomedical Technology Resource, *Developmental Resource for Biophysical Imaging Opto-Electronics (DRBIO)*, `www.drbio.cornell.edu/cross_sections.html`, [Online; accessed 21-Feb-2014].

55 L. Jia, C. Guo, L. Yang, J. Xiang, Y. Tang, C. Liu and H. Liu, *Journal of Colloid and Interface Science*, 2010, **345**, 332–7.

56 P. Desai, N. Jain, R. Sharma and P. Bahadur, *Colloids and Surfaces A: Physicochemical and Engineering Aspects*, 2001, **178**, 57–69.

57 E. B. Jørgensen, S. Hvidt, W. Brown and K. Schillén, *Macromolecules*, 1997, **30**, 2355–64.

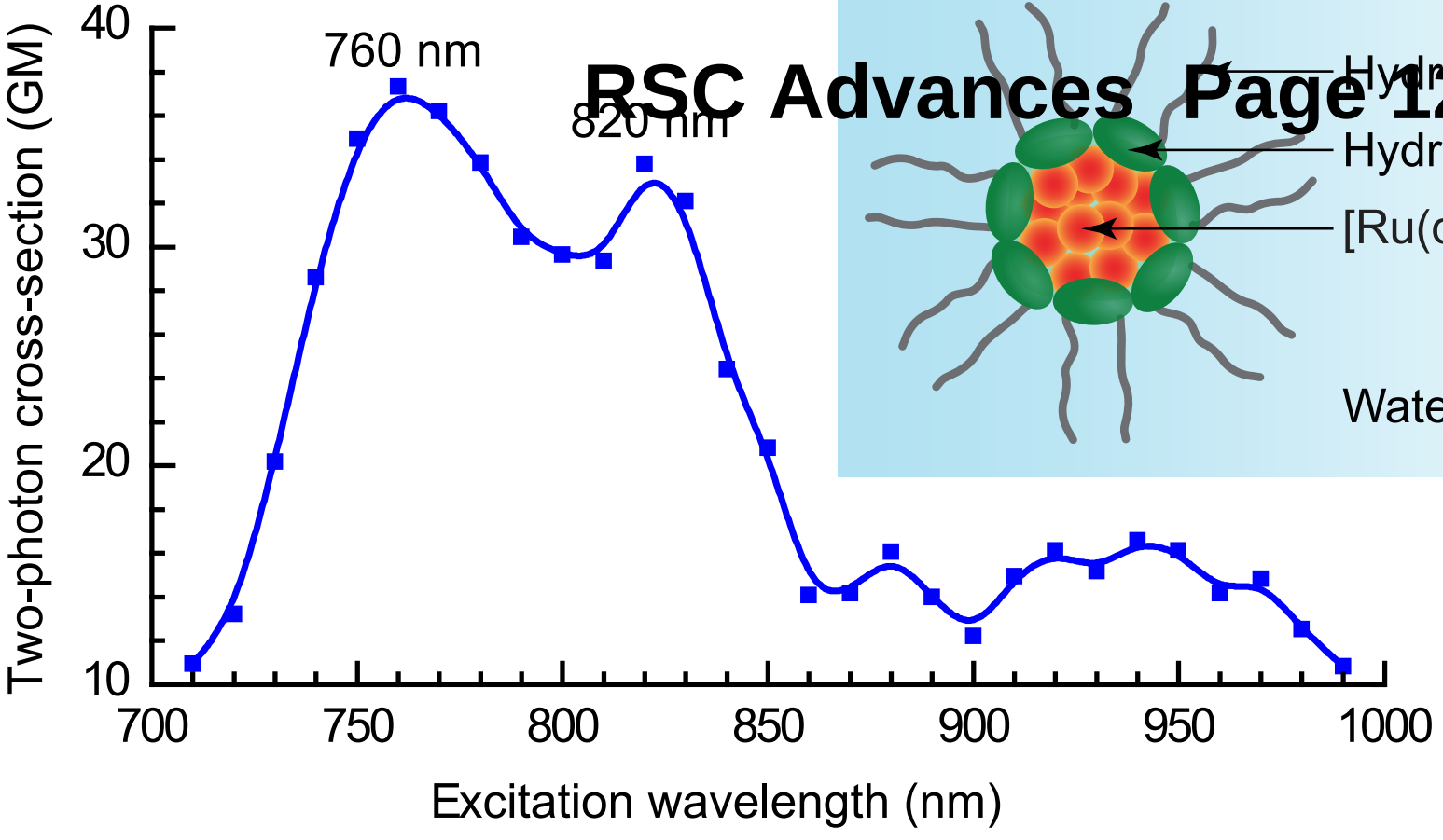

Easily prepared, biocompatible, and oxygen-sensitive optical probes with a large two-photon cross-section: towards inexpensive quantitative oxygen imaging in vivo